Journal of the Brazilian Society of Mechanical Sciences and Engineering (2018) 40:118
https://doi.org/10.1007/s40430-018-1035-6

TECHNICAL PAPER

HPHT sintering of binderless Si_3N_4: structure, microstructure, mechanical properties and machining behavior

Marcello Filgueira[1] · Águida Luzia Nery Nascimento[1] · Michel Picanço Oliveira[1] · Djalma Souza[1] · Zulmira Alice Soares Guimarães[1] · Claudinei dos Santos[2]

Received: 24 February 2017 / Accepted: 22 January 2018 / Published online: 6 February 2018

Abstract
Silicon nitride (Si_3N_4) is widely used in the manufacture of cutting tools due to the combination of properties such as high hardness, fracture toughness and wear resistance. This ceramic is usually sintered by liquid phase, causing the reduction of thermo-mechanical properties. This work investigated the sintering of pure (binderless) Si_3N_4 tools by a high pressure and high-temperature (HPHT) technology. Sub-micrometric α-Si_3N_4 powder was hot-pressed at 1700 °C for 3 min, using extreme pressures of 5, 6 or 7 GPa. The sintered samples were characterized by XRD and atomic force microscopy (AFM); hardness and fracture toughness were measured by the indentation fracture method (IF). Preliminary machining tests with binderless-Si_3N_4 tools were performed using AISI 4140 hardened steel. Commercial TiN-coated hard metal insert was used as a comparative tool material. Turning tests were carried out using coolant/lubricant, cutting time of 12 min, cutting speed of 150 m/min, cutting depth of 0.3 mm and feed of 0.11 mm/rev. The results showed the presence of α-Si_3N_4 and β-Si_3N_4 crystalline phases after sintering, indicating partial α → β phase transformation, with elongated β-Si_3N_4 grain. The relative density after sintering was near 90–97%. The best results for the mechanical properties were hardness of 21 GPa and fracture toughness of 8.9 MPa $m^{1/2}$. The machining results indicated an improvement on surface quality when using Si_3N_4 ceramic tool. The flank wear of the hard metal insert was 0.7 mm, while the wear of binderless Si_3N_4 insert was substantially lower, 0.1 mm. The roughness (R_a) measured in AISI 4140 steel was 17.6 µm (HPHT Si_3N_4 insert) and 19.7 µm (TiN-coated hard metal insert), after machining tests.

Keywords Si_3N_4 ceramics · High-pressure and high-temperature (HPHT) · Mechanical properties · Machining

1 Introduction

Silicon nitride, Si_3N_4-based ceramics can be used as structural materials due to its high flexural strength and fracture toughness, high hardness, excellent wear resistance and low creep deformation up to 1300 °C [1–5]. They are promising options for cutting tools and, therefore, have been increasingly studied over the last years [6]. One key issue of high-quality and reliable structural Si_3N_4-ceramics is to reach a high fracture toughness. This can be achieved by the combination of several factors, such as high-quality starting powders, optimization of the processing parameters that reduce the size and amount of defects. Moreover, the production of high aspect ratio grains and control of the interfacial bonding strength between the β-Si_3N_4 grains and the secondary intergranular phase can also contribute [7–10].

Si_3N_4 crystallizes in two different allotropic forms: α-Si_3N_4 and β-Si_3N_4. The α-Si_3N_4 phase is stable at room temperature, and it is characterized by its equiaxed grains. Above 1400 °C, the β-Si_3N_4 phase becomes stable. However, this transformation is difficult due to the low diffusivity of this ceramic, resulting from the covalent character of its chemical bonds. Therefore, the use of sintering additives is of utmost importance, because they form a

Technical Editor: Márcio Bacci da Silva.

✉ Marcello Filgueira
marcello.filgueira@pq.cnpq.br

[1] Universidade Estadual do Norte Fluminense-UENF/CCT/LAMAV, Av. Alberto Lamego, 2000, Campos dos Goytacazes, RJ ZIP.28013-602, Brazil

[2] Universidade do Estado do Rio de Janeiro-UERJ/FAT, Rodovia Presidente Dutra km 298, Polo Industrial de Resende, Resende, RJ ZIP.27537-000, Brazil

liquid phase above 1400 °C, which leads the sintering mechanism of dissolution–reprecipitation [1, 2, 7, 8, 10, 11] to accelerate the phase transformation. This process allows the formation of the β-Si_3N_4 phase, which remains metastable after sintering. Also, the use of high sintering temperatures and considerable isotherm levels (up to 6 h) is essential to enable this transformation.

The advantages of the β-Si_3N_4 phase focus mainly on the morphology of β-grains, with elongated format, of high aspect ratio (length to diameter). This characteristic allows better densification of the ceramic and provides excellent mechanical properties such as high fracture toughness, of the order of 6–10 MPa $m^{1/2}$, and high flexural strength of 500–800 MPa [1, 2, 7, 12–14].

Initially, α-Si_3N_4 was sintered conventionally, without the use of additives or pressure [10, 14–16]. In this process, high temperatures of the order of 1900–2100 °C, in addition to long isotherm holding times, are required to obtain the complete densification of this ceramic [17]. However, previous studies [14] report the abnormal growth of β-Si_3N_4 grains and partial decomposition of this phase, causing an increase in the residual porosity of the sintered body and reducing its mechanical properties. Ziegler et al. [14] investigated the production of dense Si_3N_4 using the reactive sintering technique. As a major problem, the authors observed a great microstructural heterogeneity, reducing the reproducibility in the properties of this ceramic.

Sintering additives, such as Y_2O_3 (or mixture of rare earth oxides) and Al_2O_3, are usually mixed withα-Si_3N_4 particles which possess surface layers of silica. The rare earth oxides and Al_2O_3 react with this silica and with some of the silicon nitride itself at sintering temperatures to form liquid oxynitride, which promotes densification by solution–precipitation [7, 8, 17, 18].

Among the sintering techniques for silicon nitride, liquid phase sintering has been used to obtain Si_3N_4 with high bending strength, fracture toughness and high hardness. This process is carried out at 1750–1900 °C under a nitrogen atmosphere (0.1–10 MPa) [1, 2, 10, 16–18].

Nevertheless, there is a disadvantage in using sintering additives: during sintering, these additives are converted into an amorphous or partially crystallized intergranular phase, which considerably reduces the hardness and thermo-mechanical properties of the silicon nitride ceramic. Hence, some technological applications, such as machining tools, are partially compromised.

Due to the potential use of this ceramic, several liquid phase sintering processes have been studied such as uniaxial hot pressing (HP) [18–20], using pressures up to 100 MPa, hot isostatic pressing (HIP), using pressures up to 400 MPa [21], microwave sintering [22] and spark plasma sintering (SPS) [23], among others. As common feature, all these techniques reveal the presence of residual intergranular phase among the β-Si_3N_4 grains. However, to the best of our knowledge, there are no reports of binderless Si_3N_4 sintering using pressures at the gigapascal scale (GPa), and thus the effect of this pressure scale on densification and α → β-Si_3N_4 transformation.

The high-pressure and high-temperature sintering technique (HPHT) [24–26] uses pressure in GPa scale, to obtain densification and refractory metal and ceramics, aiming to obtain super hard materials. This technique has been used with great success for the manufacture of components such as synthetic diamond and cubic boron nitride, at temperatures of the order of 2000 °C, under pressures of the order of 5–7 GPa and at short intervals of time.

In this work, binderless Si_3N_4 ceramics were sintered using the high-pressure and high-temperature (HPHT) technique. The sintering was carried without the presence of additives, aiming at full densification, with consequent increase in fracture toughness and mechanical property improvements. It indicates that sintered material could be used in the machining of metallic alloys.

2 Experimental procedure

2.1 Samples processing by HPHT

High-purity silicon nitride powder containing 99.9 wt% α-Si_3N_4 and 0.1% Si (SN10, UBE Industries-Japan), with average particle size of 200 nm, was used. In each sample, approximately 0.275 g of Si_3N_4 powder was filled into a graphite heater chamber (mold).

After filling the mold with the Si_3N_4 powder, this mold was installed directly into deformable calcite capsules, which was assembled into cavity of hard metal anvils in a special hydraulic press (630 tons capacity) model DO138B-Ryazantyashpressmash (Russia). This equipment is used to generate maximum pressure of 8 GPa and temperatures up 1700 °C—commonly used to sinter superhard materials: diamond and cubic boron nitride. The samples were sintered fast at 1700 °C for 3 min, using three high-pressure values: 5, 6 or 7GPa.

2.2 Characterizations

The relative density of all sintered samples was determined using Archimedes' principle, correlating apparent density with theoretical density.

The crystalline phases were determined by X-ray diffraction analysis, using a Shimadzu™ XRD7000-diffractometer. The analysis was conducted using Cu–Kα radiation with Ni filter, in the 2θ range of 10–80°, a step width of 0.03° and an exposure time of 2 s per position. The peaks were identified by comparison with JCPDS files [27].

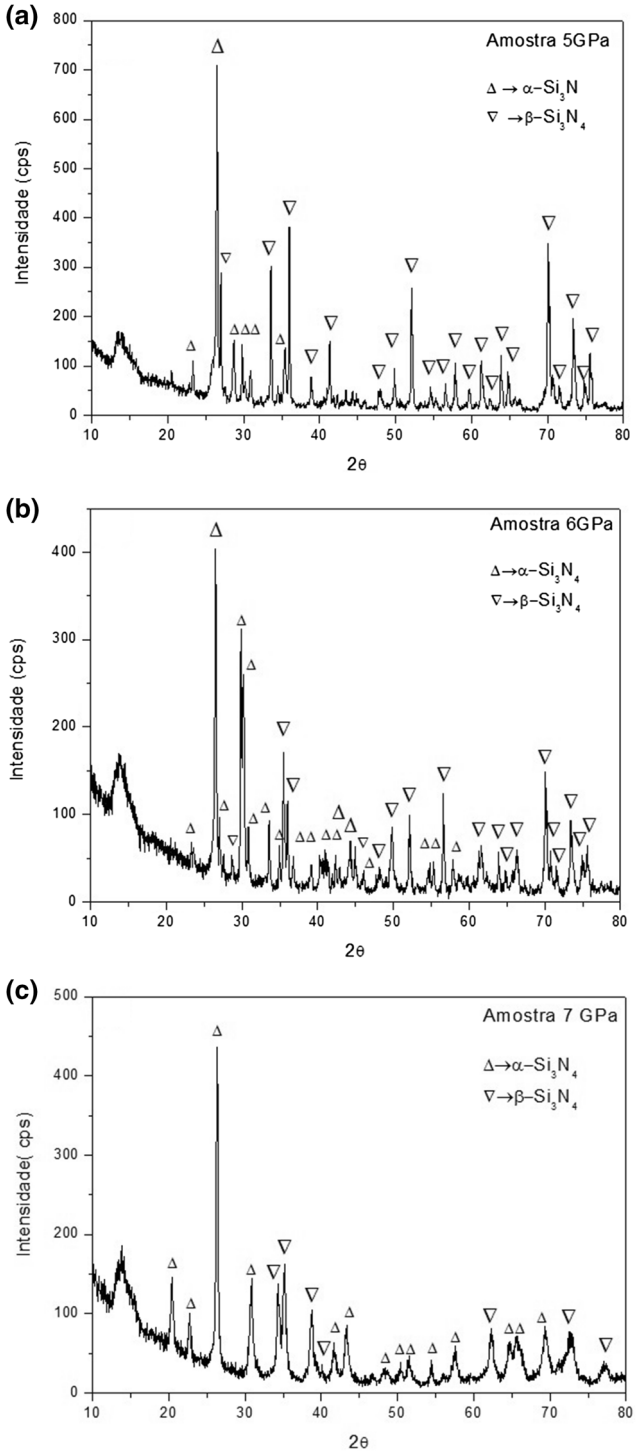

Fig. 1 XRD patterns of the Si_3N_4 sintered at 1700 °C for 3 min under pressure: **a** 5 GPa, **b** 6 GPa and **c** 7 GPa

2.2.1 Mechanical properties

For Vickers hardness and fracture toughness test, the cross sections of sintered samples were embedded in acrylic resin and the surface was polished with diamond suspension (1–3 μm). Five (05) Vickers hardness indentations per sample were made in a microhardness tester (Pantec^{TM} model RBS) with 1000 gF load for 15 s.

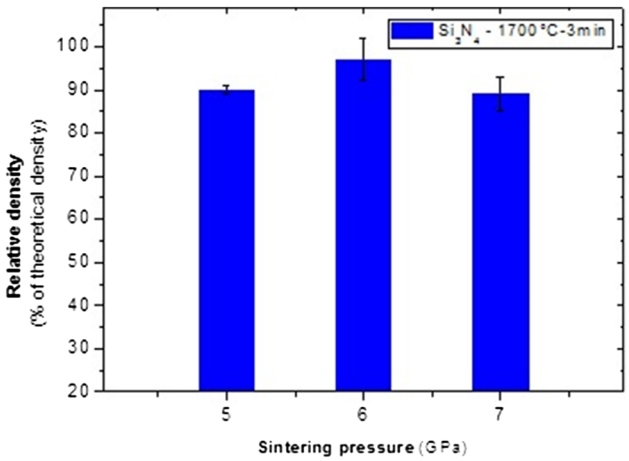

Fig. 2 Relative density of Si_3N_4 samples sintered by HPHT at 1700 °C for 3 min

Fracture toughness was determined by Vickers hardness indentation technique, which is based on the relationship among the Vickers hardness value, cracks that form from each corner of the indentation and Young's modulus. The fracture toughness, K_{IC}, was calculated using the methodology proposed by Hanyaloglu et al. [28].

2.2.2 Microstructural analysis

The Shimadzu^{TM}SuperScan/FF500-50 (with EDS coupled) Scanning Electron Microscope (SEM), was used for the visualization of microstructural features of the samples after the machining tests, to measure the flank wear length and to observe crack propagation.

A MultiMode model atomic force microscope (AFM0) was employed to identify the presence of phases α-Si_3N_4 and β-Si_3N_4, in the sintered samples and to observe the aspect of grains (morphology and aspect ratio).

2.2.3 Machining tests

The sintered Si_3N_4 was fixed in tool holders and then attached to the lathe ROMI-TORMAX 20A. Cylindrical samples measuring 4.5 mm diameter × 5 mm height and back rake angle of 45° were used.

Pure Si_3N_4 was subjected to the test of wear by machining a piece of AISI4140 steel with cylindrical shape and internal and external diameters of 45 and 90 mm, respectively. The wear condition was assessed in terms of mass loss of Si_3N_4 in external turning operations of the piece of steel AISI 4140 hardened and tempered to 58–60 HRC.

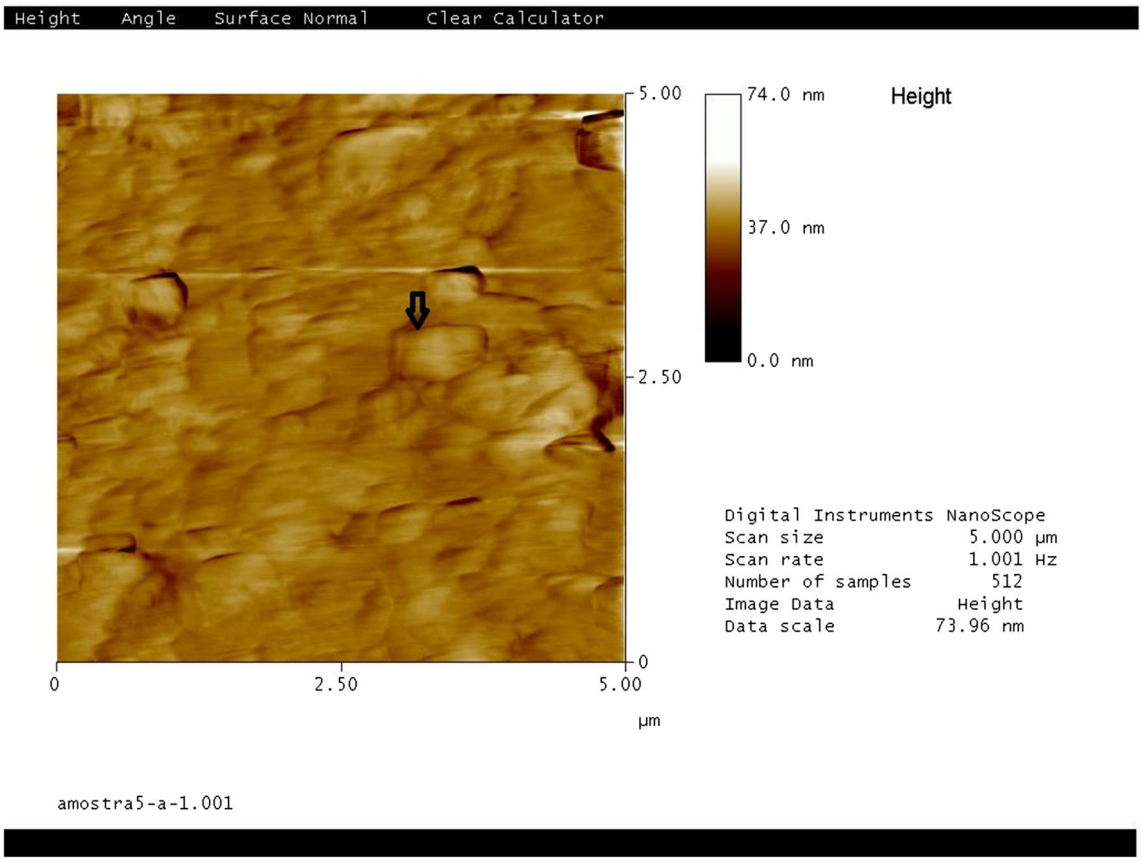

Fig. 3 AFM of Si_3N_4 binderless ceramic, sintered at 1700 °C for 3 min (5 GPa)

Turning tests were performed using Emulsol as coolant/lubricant, adopting the parameters: cutting time of 12 min, cutting speed of 150 m/min, cutting depth of 0.3 mm and feed 0.11 mm/rev, in accordance with Bobrovnitchii and Filgueira [24]. These parameters were used in the machining of the same steel using boron wurtzite nitride—also called Hexanite-R, Amborite and hard metal commercial inserts.

The AISI 4140 steel piece was also machined with a commercial TiN-coated hard metal insert—using the same cutting parameters for Si_3N_4, aiming to compare the results.

2.2.4 Workpiece surface after machining tests

A laser confocal microscope Lext Olympus OLS4000 was used to observe the microstructural features of the turned AISI4140 hardened steel. This microscope is equipped with a laser scanning system, which measures the surface roughness at the non-contact mode.

3 Results and discussion

3.1 Characterization of HPHT sintered samples

The X-ray diffraction (XRD) patterns of sintered samples are shown in Fig. 1.

The analysis of the XRD patterns (Fig. 1) reveals that the ceramics sintered at 1700 °C for 3 min and the α-Si_3N_4 and β-Si_3N_4 present as crystalline phases, regardless of the sintering pressure applied during the densification process. This is due to the characteristics of the $\alpha \rightarrow \beta$ phase transformation, which is strongly dependent on the presence of a liquid phase to activate the phase transformation mechanisms [7]. The low diffusivity and the reduced sintering time of 3 min, used in this work, were not sufficient for completing the $\alpha \rightarrow \beta$ Si_3N_4 phase transformation.

On the other hand, it is possible to affirm that the high pressures to which the Si_3N_4 was subjected during the heat treatment act as driving force for the beginning of the $\alpha \rightarrow \beta$ phase transformation, even in the solid state and

without the presence of the liquid phase (additives). This may be due to the chemical interaction between α-Si_3N_4, unstable above 1400 °C, and the thin layer of SiO_2, notably present in α-Si_3N_4 particles, as already discussed in several previous works [2, 7, 8]. Due to the high pressure at which they are subjected, these accelerate the localized dissolution–reprecipitation and favor the α → β transformation. More detailed studies should be carried out evaluating the effect of sintering time on α → β-Si_3N_4 transformation during HPHT sintering.

The relative density results of HPHT Si_3N_4 samples sintered at 1700 °C for 3 min are shown in Fig. 2.

The results indicate that the samples sintered by HPHT present relative densities between 89 and 97%. In contrast to the use of sintering additives, samples of binderless Si_3N_4 reached high densification at an usual intermediate sintering temperature of Si_3N_4, 1700 °C, with extremely reduced isothermal times (3 min).

This short isotherm time is important to prevent grain growth or thermal decomposition of Si_3N_4 and is motivated by high sintering pressures. It is observed that the increase of the pressure leads to an increase of the relative density in pressures of up to 6 GPa, reaching 97% of relative density. By using sintering pressure of 7 GPa, the densification is dramatically reduced. This in explained by the presence of a large amount of cracks generated by this pressure increment, also compromising the mechanical properties.

The results obtained are extremely satisfactory, when compared with those of literature—where the liquid phase sintering technique is adopted in the latter: as examples, Matovic Bocanegra–Bernal [29] obtained the density ranges from 86 to 100% after several sintering techniques, with temperatures between 1500 and 1825 °C; Huang et al. [30], using a pulsed electric current sintering, obtained full density at 1650 °C [18].

AFM Microstructural characterization of typical Si_3N_4 sintered at 1700 °C for 3 min (5 GPa) is shown in Fig. 3. A microstructure with very fine grains is observed. A black arrow points to a hexagonal grain—along the plane system {0001}. This may be an evidence of the transformation of α- to β-phase. It seems that the applied high pressure along with a very short sintering time suppressed Si_3N_4 grain growth.

Microstructures from a crack are depicted in Fig. 4a–c. These cracks were generated by the applied high pressure of 5 GPa during the short sintering process. The presence of a duplex microstructure formed of β-Si_3N_4 elongated grains and α-Si_3N_4 equiaxed grains confirming the results shown in Fig. 1 can be observed.

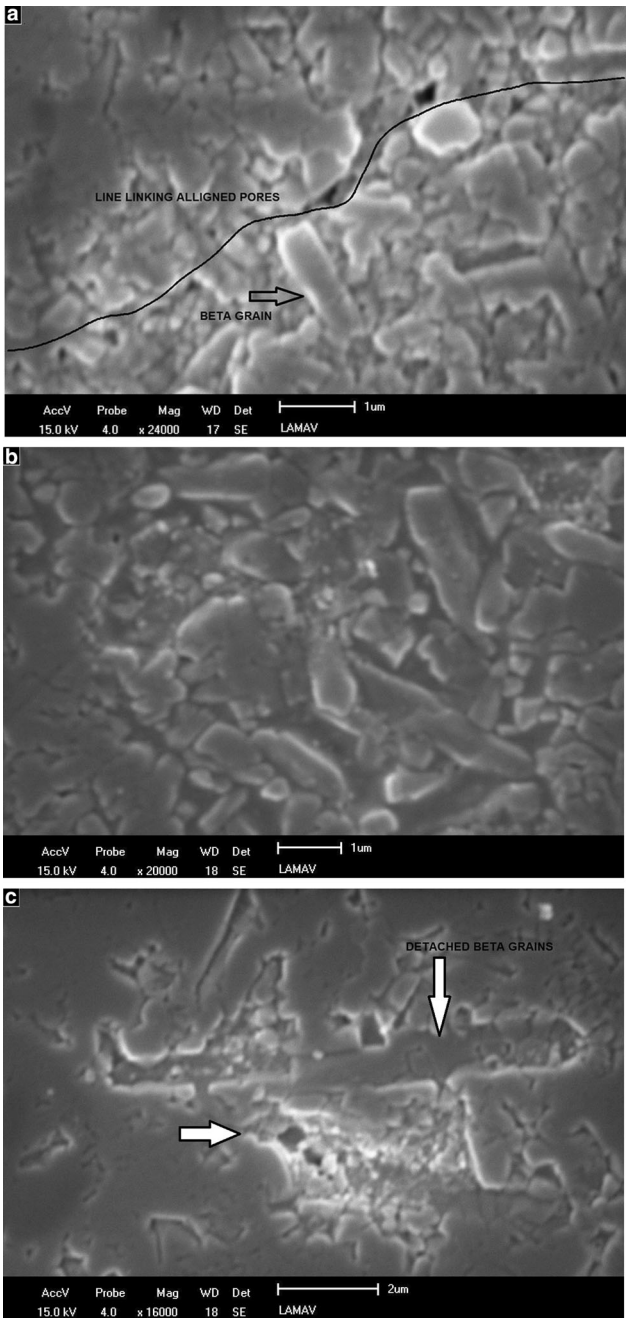

Fig. 4 Typical microstructure of binderless Si_3N_4 HPHT sintered sample (1700 °C for 3 min): **a** half portion of a crack; **b** quarter half portion of a crack; **c** end portion of a crack—high pressure induced (sample sintered at 5 GPa)

The half portion of the crack is shown in Fig. 4a. The curved line accompanies the path of the crack growth—one can observe the aligned nano-sized pores, which weaken the microstructure, justifying the presence of the crack

Table 1 Mechanical properties of HPHT sintered Si_3N_4 samples

Sintering condition	Sintering pressure	Relative density (% TD)	Crystalline phases	Hardness (HV_{1000gF}) (GPa)	Fracture toughness (K_{IC}) (MPa $m^{1/2}$)
1700 °C–3 min (HPHT)	5 GPa	90 ± 2	β-Si_3N_4	14.2 ± 1.8	9.94 ± 1.09
	6 GPa	97 ± 5	and α-Si_3N_4	21.3 ± 2.0	8.86 ± 0.55
	7 GPa	89 ± 4		15.9 ± 7.6	9.61 ± 0.37

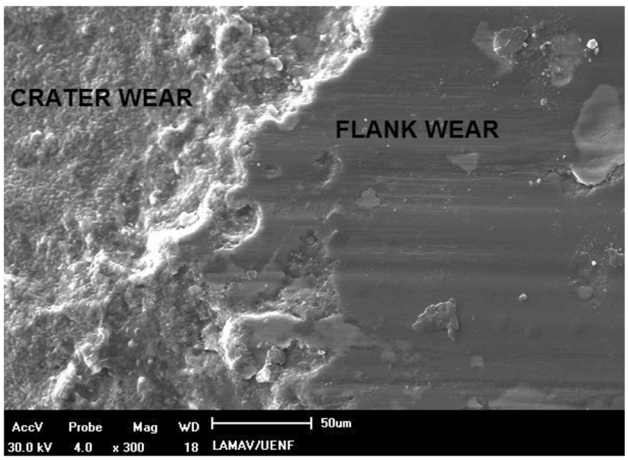

Fig. 5 SEM image of HPHT sintered sample (1700 °C-min, 5 GPa) with flank wear and crater types of abrasion, after the turning test

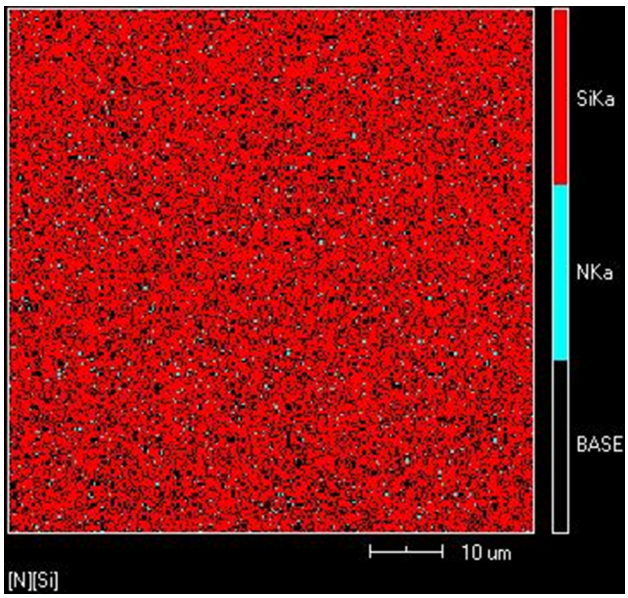

Fig. 6 EDS mapping of the flank wear region of Fig. 5

there. An elongated grain is seen at the center of the micrograph, which is probably a β-phase grain (see black arrow).

The aspect of the crack at a quarter half to its end is shown in Fig. 4b. A large amount of β-elongated grains are visible, mainly at the center of the micrograph. Some of them were pulled out. The end region of the crack is shown in Fig. 4c. A plane and dense microstructure is observed, and a region of detached β-phase grains is clear at the central region of the micrograph. The black arrow points to the end of the crack tip. This is an indication of the active toughening mechanism of Si_3N_4 ceramic materials by α–β phase transformation, where the elongated hexagonal β grains deflect or even block the cracks. In this case, Fig. 4a, b shows β-elongated grains deflecting the crack. On the other hand, Fig. 4c shows an array of detached β grains that blocked the tip of the crack.

3.2 Mechanical properties

The results of hardness and fracture toughness of sintered samples are presented in Table 1.

Hardness results indicate high values, between 14 and 21 GPa, and they are consistent with the relative density of samples sintered by HPHT. Compared with the results obtained in sintered ceramics by the liquid phase, the results are sensitive to the porosity and intergranular phase content. Huang et al. [30] and Tatli et al. [31] sintered Si_3N_4 ceramics by conventional techniques, using sintering additives. The hardness values range from 9.7 to 18.4 GPa, for Si_3N_4 ceramic sintered between 1400 and 1750 °C. Yang et al. [32]. obtained a hardness of 16.5 HV for a low pressure-assisted silicon nitride sintering at 1800 °C.

The results of fracture toughness indicate that the ceramics present high K_{IC} between 8.5 and 10 MPa $m^{1/2}$, even without the presence of intergranular phase, and motivate its use as a cutting tool. Tatli et al. [18], when studying sintering-aided Si_3N_4, found fracture toughness ranging from 4.2 to 5.3 MPa $m^{1/2}$. According to data reported by Tapasztó et al. [33], the fracture toughness values vary between 2 and 5 MPa $m^{1/2}$. Furthermore, Yang et al. [34] found a value of 7.2 MPa $m^{1/2}$ for low pressure-assisted sintering of Si_3N_4 using Y_2O_3 or La_2O_3 as sintering additives.

Table 2 Roughness of AISI4140 steel after turning tests

Material	Machining test conditions	Roughness (R_a) μm
HPHT binderless Si_3N_4 insert (1700 °C-3 min, 5GPa)	Using coolant/lubricant, cutting time: 12 min, speed: 150 m/min, cutting depth: 0.3 mm, feed 0.11 mm/rev	17.60 ± 2.58
Commercial TiN-coated hard metal insert		19.70 ± 3.89

The high fracture toughness can be attributed to several factors, such as the increase of the relative density, the α-to-β-Si_3N_4 transformation, but mainly due to microstructural aspects. The reduction of porosity influenced the fracture toughness due to the reduction of the amount and size of defects. The high fracture toughness is explained by the microstructure consisting of elongated grains with high aspect ratio, which act as crack propagation barriers, increasing the energy consumed during crack growth. In the ceramics sintered in this work, the main toughening mechanisms are crack bridging and crack deflection [2, 9, 34].

3.3 Machining tests

The topography of an Si_3N_4 tool surface after machining is shown in Fig. 5. It can be seen that the main wear mechanism was abrasion—denoted by crater and flank wear modes, since there was no spread of machined material in the cutting tool.

The EDS mapping carried out in the region of flat surface (flank) in Fig. 5 was performed and the presence of only Si and N was observed, along with their good distribution, without the presence of iron (Fe)—see Fig. 6. This means that there was no diffusion wear, which leads to an increased tool performance and lifetime.

3.4 Tribological analysis

The roughness of the cylindrical AISI4140 steel samples submitted to the turning tests, using HPHT binderless Si_3N_4 insert or, comparatively, TiN-coated hard metal insert, is shown in Table 2.

It can be observed that there was a remarkable difference between the workpiece surface (steel) when machined with the binderless Si_3N_4 tool and commercial TiN-coated hard metal insert. This fact describes the surface quality improvement when using the Si_3N_4 ceramic. The flank wear of the hard metal insert was 0.7 mm and the wear of Si_3N_4 cylinder was substantially lower, 0.1 mm measured by SEM and laser confocal microscopy. This indicates a higher performance and increased lifetime for the HPHT sintered pure Si_3N_4 samples.

Confocal laser microscopy surface images of AISI4140 steel parts and their roughness profiles after machining tests with different tools are shown in Fig. 7. It is possible to observe more continuous and cracks-free surfaces, with closer grooves for the surface turned with the HPHT binderless Si_3N_4 insert, rather than when using the commercial TiN-coated hard metal.

Binderless Si_3N_4 flank wear (100 μm) was 2.8 times lower than that found by Long et al. [34], using similar turning parameters—flank wear: 280 μm, when turning an AISI4340 steel (hardened to 52 HRC—same order of magnitude of the AISI4140) with Si_3N_4 sintered with additives insert (16 HV and 5 MPa $m^{1/2}$). One can attribute this result to the use of binderless Si_3N_4, and it seems to be a fruitful achievement, over the novelty that is the possibility to obtain silicon nitride dense bodies with good properties.

4 Conclusions

According to this study, promising results were achieved regarding the sintering of advanced high strength ceramic materials, resulting in the possibility of using the HPHT special processing route to obtain dense binderless silicon nitride bodies. It presents the following main findings:

1. In general, densification was satisfactory in all parameters used, reaching about 80% up to 97% density.
2. Good hardness values were achieved, the highest was 21 HV for samples sintered with a pressure of 6 GPa.
3. The fracture toughness results are between 8 and 10 MPa $m^{1/2}$ for samples of three groups, which are excellent when compared with conventionally sintered bonded Si_3N_4, considering that fracture toughness is a very important mechanical property to ensure a satisfactory tool lifetime and performance.
4. The structural analyses by X-ray diffraction showed that the phase transformation α → β was achieved.
5. Atomic force microscopy showed the presence of α and β phase and a very fine microstructure after sintering.
6. The machining tests were performed only with 5 GPa samples. The main features were the presence of flank wear and crater formation, and the absence of iron diffusion, indicating the abrasion wear mechanism. The surface quality generated by the processed Si_3N_4

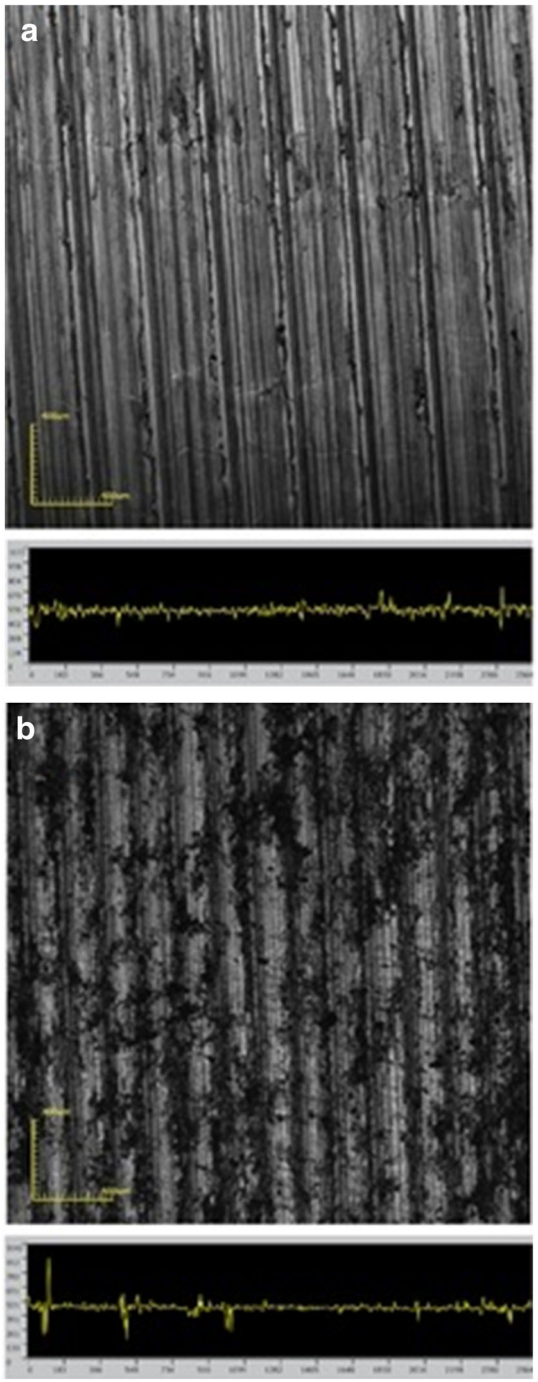

Fig. 7 Confocal laser microscopy of the workpiece's surface, also showing the roughness profile, after the turning tests: **a** using commercial hard metal insert; **b** using HPHT(1700 °C for 3 min, 5GPa) binderless Si_3N_4 insert (magnification × 108)

cylinder was better than that obtained when using a commercial TiN-coated hard metal insert, employing the same turning parameters. Si_3N_4 was far more wear resistant than the commercial hard metal insert.

7. Binderless silicon nitride presented lower flank wear than the conventional silicon nitride inserts, sintered with the aid of additives.

Acknowledgements The authors would like to express their gratitude to the Brazilian agencies CNPq and FAPERJ. The authors are indebted to Mr. Renan da Silva Guimarães, who sintered all the samples by HPHT.

References

1. Riley FL (2000) Silicon nitride and related materials. J Am Ceram Soc 83(2):245–265
2. Lange FF (2006) The sophistication of ceramic science through silicon nitride studies. J Ceram Soc Jpn 114:873–879
3. Santos C, Strecker K, Baldacim SA, Silva OMM, Silva CRM (2003) Mechanical properties improvement related to the isothermal holding time in Si_3N_4 ceramics sintered with an alternative additive. Int J Refract Metal Hard Mater 21(5–6):245–250
4. Luecke WE, Widerhorn SM, Hockey BJ, Krause RF, Long GG (1995) Cavitation contributes substantially to tensile creep in silicon nitride. J Am Ceram Soc 78(8):2085–2096
5. Strecker K, Gonzaga R, Ribeiro S, Hoffmann MJ (2000) Substitution of Y2O3 by a rare earth oxide mixture as sintering additive of Si_3N_4 ceramics. J Mater Sci Lett 45:39–42
6. Dante RC, Kajdas CK (2012) A review and a fundamental theory of silicon nitride tribochemistry. Wear 288:27–38
7. Hampshire S, Pomeroy MJ (2012) Grain boundary glasses in silicon nitride: a review of chemistry, properties and crystallisation. J Eur Ceram Soc 32:1925–1932
8. Kleebe H-J, Pezzotti G, Ziegler G (1999) Microstructure and fracture toughness of Si_3N_4 ceramics: combined roles of grain morphology and secondary phase chemistry. J Am Ceram Soc 82(7):1857–1867
9. Becher PF, Sun EY, Plucknett KP, Alexander KB, Hsueh C-H, Lin HT et al (1998) Microstructural design of silicon nitride with improved fracture toughness: I. Effects of grain size and shape. J Am Ceram Soc 81(11):2821–2830
10. Kingery WD (1959) Densification during sintering in the presence of a liquid phase I. Theory. J Appl Phys 30:301–306
11. Suttor DS, Ischman GS (1992) Densification and sintering kinetics in sintered silicon nitride. J Am Ceram Soc 75:1063–1067
12. Santos C, Strecker K, Baldacim SA, Silva OMM, Silva CRM (2004) Influence of additive content on the anisotropy in hot-pressed Si_3N_4 ceramics using grain orientation measurements. Ceram Int 30(5):653–659
13. Becher PF (1991) Microstructural design of toughened ceramics. J Am Ceram Soc 74(2):255–269
14. Ziegler G, Heinrich J, Wotting G (1987) Relationships between processing, microstructure and properties of dense and reaction-bonded silicon nitride. J Mater Sci 22:3041–3086
15. Díaz A, Hampshire S (2004) Characterization of porous silicon nitride materials produce with starch. J Eur Ceram Soc 24(2):413–419
16. Hampshire S, Jack KH (1981) The kinetics of densification and phase transformation in nitrogen ceramics. Proc Brit Ceram Soc 31:37–49
17. Santos C, Strecker K, Baldacim SA, Silva OMM, Silva CRM (2003) Mechanical properties improvement related to the isothermal holding time in Si_3N_4, ceramics sintered with an

alternative additive. Int J Refract Metals Hard Mater 21(5–6):245–250
18. Lukianova OA, Krasilnikov VV, Parkhomenko AA, Sirota VV (2016) Microstructure and phase composition of cold isostatically pressed and pressureless sintered silicon nitride. Nanoscale Res Lett 11(1):148
19. Mengyong S, Qinggang L, Shifeng H, Xin C (2015) Fabrication and properties of C fiber/Si_3N_4 composite by vacuum hot-pressing sintering. Ceram Int 41(4):6084–6088
20. Santos C, Strecker K, Barboza MJR, Piorino Neto F, Silva CRM (2005) Compressive creep behavior of hot-pressed Si_3N_4 ceramics using alumina and a rare earth solid solution as additives. Int J Refract Metals Hard Mat 23(3):183–192
21. Gu H, Cannon RM, Tanaka I, Rühle M (2006) Calcia partition in phase-separated intergranular glass and interfaces in doped silicon nitride produced by hot isostatic pressing. Mater Sci Eng A 422(1):51–65
22. Zgalat-Lozinskii O (2015) Structure of Si_3N_4–Y_2O_3–Al_2O_3 and TiN–AlN composites consolidated in microwaves (2.45 GHz). Powder Metall Met Ceram 54(1):60–66
23. Li JL, Chen F, Niu JY (2011) Low temperature sintering of Si_3N_4 ceramics by spark plasma sintering technique. Adv Appl Ceram 110(1):20–24
24. Bobrovnitchii GS, Filgueira M (2005) Study of quenched steels machining with a polycrystalline Hexanite-R cutting tool. J Mater Process Technol 170:254–258
25. Bobrovnitchii GS, Osipov OS, Filgueira M (2003) Some peculiarities of the diamond micro-powder sintering. Int J Refract Metal Hard Mater 21:251–258
26. Eko A, Fukunaga O, Naoto Ohtake N (2015) High pressure sintering of cubic boron nitride using Co–V–Al alloy as bonding media. Int J Refract Metal Hard Mater 50:178–183
27. JCPDS Powder Diffraction File (2010) Inorganic materials. International Centre for Diffraction Data, Swarthmore
28. Hanyaloglu C, Aksakal B, Bolton JD (2001) Production and indentation analysis of WC/Fe-Mn as an alternative to cobalt bonded hardmetals. Mater Charact 47:315–322
29. Bocanegra-Bernal MH, Matovic B (2009) Dense and near-net-shape fabrication of Si_3N_4 ceramics. Mater Sci Eng A 500:130–149
30. Huang S, Swarnakar AK, Vanmeesel K, Vleugels J (2013) Diamond dispersed Si_3N_4 composites obtained by pulsed electric current sintering. Int J Refract Matals Hard Mater 51:451–462
31. Tatli Z, Çaliskan F, Butler J, Crowley C, Hampshire S (2014) SPS sintering of silicon nitride with fluoride additive. Ceram Int 40:1399–1404
32. Yang X-F, Yang J-H, Xu X-W, Liu Q-C, Xie Z-P, Liu W (2015) Injection molding of ultra-fine Si_3N_4 powder for gas-pressure sintering. Int J Miner Metall Mater 22(6):654–659
33. Tapasztó O, Kun P, Wéber F, Gergely G, Balázsi K, Pfeifer J, Arató P, Kidari A, Hampshire S, Balázsi C (2011) Silicon nitride based nanocomposites produced by two different sintering methods. Ceram Int 37:3457–3461
34. Long Y, Zeng J, Shanghua W (2014) Cutting performance and wear mechanism of Ti–Al–N/Al–Cr–O coated silicon nitride ceramic cutting inserts. Ceram Int 40(7):9615–9620